Variable pressure JSR study of low temperature oxidation chemistry of n-heptane by synchrotron photoionization mass spectrometry

Weiye Chen, Qiang Xu, Hao Lou, Qimei Di, Cheng Xie, Bingzhi Liu, Jiuzhong Yang, Hervé Le Gall, L.S. Tran, Xudi Wang, et al.

Variable pressure jet-stirred reactor to study low-temperature oxidation chemistry of *n*-heptane by synchrotron photoionization mass spectrometry

Weiye Chen [a], Qiang Xu [a], Hao Lou [a], Qimei Di [a], Cheng Xie [a], Bingzhi Liu [a], Jiuzhong Yang [a *], Hervé Le Gall [b,c], L. S. Tran [b,c], Xudi Wang [d], Zongyu Xia [d], Olivier Herbinet [b,c], Frédérique Battin-Leclerc [b,c *], Zhandong Wang [a,e,f *]

[a] *National Synchrotron Radiation Laboratory, University of Science and Technology of China, Hefei, Anhui 230029, PR China*

[b] *Laboratoire Réactions et Génie des Procédés, CNRS UMR 7274, Ecole Nationale Supérieure des Industries Chimiques, 1 rue Grandville, 54000 Nancy*

[c] *Laboratoire Réactions et Génie des Procédés, Université de Lorraine, Ecole Nationale Supérieure des Industries Chimiques, 1 rue Grandville, 54000 Nancy*

[d] *School of Mechanical Engineering, Hefei University of Technology, 193 Tunxi Rd., Hefei 230009, China*

[e] *State Key Laboratory of Fire Science, University of Science and Technology of China, Hefei, Anhui 230026, PR China*

[f] *Dalian National Laboratory for Clean Energy, Dalian 116023, China*

Published in Combustion and Flame

https://doi.org/10.1016/j.combustflame.2021.111946

Abstract

The low-temperature oxidation chemistry is crucial in the auto-ignition process of the internal combustion engines. The development of laboratory based reactor and diagnostic systems promotes our understanding of the low-temperature oxidation mechanism. In this work, we developed a variable pressure jet-stirred reactor (VP-JSR) platform working from 1 to 10 bar. Compared to previous high pressure work that routinely use gas chromatography to analyze the

[*] Corresponding author e-mails: jzhyang@ustc.edu.cn (J. Yang), frederique.battin-leclerc@univ-lorraine.fr, (F. Battin-leclerc), zhdwang@ustc.edu.cn (Z. Wang)

low-temperature oxidation products, the novelty of this work is the possibility of probing intermediates by synchrotron vacuum ultraviolet photoionization mass spectrometry via a molecular beam sampling. The setup was validated by repeating *n*-heptane low-temperature oxidation experiments at 1 and 10 bar, respectively. A good agreement was observed between the data in this work and the data in the literature. Compared to the literature study, a much more detailed species pool was probed, including H_2O_2, carbonyl acids, alkylhydroperoxides, and keto-hydroperoxides. As a first demonstration of the usefulness of this setup, the low-temperature oxidation of *n*-heptane with initial fuel mole fraction of 0.005, residence time of 2 s, and equivalence ratio of 1.0 was studied at 1, 5, and 10 bar. The preliminary results including the reactants, final products, and the initial low-temperature oxidation intermediates are discussed. The VP-JSR system developed in this work is valuable to study the fuel chemistry from 1 to 10 bar, to develop and examine the chemical kinetic models, and to guide the development of the reaction system at even higher pressure, like those at the engine working conditions and supercritical conditions.

Keywords: autoxidation; peroxides; kinetic modeling; synchrotron radiation photoionization mass spectrometry

1. Introduction

Investigating low temperature oxidation chemistry of hydrocarbons and alternative fuels is prerequisite to improving the efficiency of internal combustion engines, and developing new concepts for combustion engines and their fuels [1,2]. Laboratory based reaction systems, such as flow reactors (FR) [3,4], shock tubes (ST) [5], rapid compression machines (RCM) [6], and jet-stirred reactors (JSR) [7,8] are commonly used to examine the low temperature oxidation chemistry of fuels. Because of the well-defined physical properties and 0-D structure for simulation, the JSRs were coupled to various analytic tools that contributed significantly to exploring the low temperature oxidation mechanism and providing speciation data for kinetic model development [7,9,10].

The JSR systems that are used by several labs in the combustion community are presented in Table 1. The JSR system currently being used functions at the pressure range of one to 40 bar. Recent work by Zhao et al. [11] developed a supercritical pressure JSR that can work at 100 bar. The analytic methods include gas chromatography (GC) with a flame ionization detector (FID), a thermal conductivity detector (TCD) and a mass spectrometer detector, Fourier transform Infrared spectroscopy (FTIR), cavity ring down spectroscopy (CRDS), and mass spectrometry (MS). The GC and FTIR can analyze stable products, while the CRDS method detects H2O2 and HO2 radical [12,13]. The mass spectrometry system used can be categorized into two groups, according to the ionization source. The first group adopts photoionization like the synchrotron vacuum ultraviolet photoionization (SVUV-PI) with tunable photon energy from 7 – 20 eV [10], and single photoionization (SPI) with fixed photon energy of 10.5 eV [14]. The time-of-flight mass spectrometer (TOF-MS) with a mass resolution from 1000 to 5000 is commonly used at the Hefei Light Source [15], Advanced Light Source [16], and LRGP-CNRS [14]. Another group used chemical ionization coupled with a high mass resolution mass spectrometer (HRMS) such as the orbitrap mass spectrometer with mass resolution higher than 100,000, like the systems with

atmospheric pressure chemical ionization (APCI) used at KAUST [17,18] and ICARE-CNRS [19,20]. Moreover, recent work by Battin-Leclerc et al. [21,22] coupled a JSR to a double imaging photoelectron photoion COincidence (i^{2}PEPICO) scheme at the DESIRS beamline of SOLEIL. The coincident mass-tagged threshold photoelectron spectra (TPES) produced better identification of low temperature oxidation intermediates.

Table 1. The typical JSR systems used in the combustion community

Research Team	JSR volume (cm^3)	Working pressure (bar)	Analytic method	Reference
ICARE-CNRS	35	1-40	GC/FTIR	[23,24]
	37	1	CRDS	[13]
	35	10	APCI-Orbitrap MS	[19,20]
LRGP-CNRS	85	1	GC/FTIR	[7,25]
	85	1	CRDS	[12,26]
	85	1	SPI-MS	[14,27]
	65.4	1-10	GC	[28,29]
KAUST	76	1	GC	[30]
	76	1	CI-Orbitrap MS	[17,18]
ALS	33.5	1	SVUV-PIMS	[16,31,32]
NSRL	102	1	SVUV-PIMS	[15,33]
SOLEIL	60	1	PEPICO	[21,22]
IET-CAS	65	1	GC	[34]
SJTU	103	1	GC	[35]
XJTU	87	1	GC	[36,37]
Princeton	0.5	100	GC	[11]

Previous studies have shown that the JSR, coupled with synchrotron vacuum ultraviolet photoionization mass spectrometry (SVUV-PIMS), is sufficiently powerful to reveal species distribution and reaction mechanisms of low temperature oxidation chemistry, especially complex oxygenated intermediates with carbonyl, carboxy, and peroxy groups [8,10]. Currently, only the JSR system at one bar is coupled to the SVUV-PIMS system. Recent studies by Dagaut et

al. [19,20,38] analyzed low temperature oxidation intermediates from the high pressure JSR at ten bar. Products were collected in a trap, separated by high performance liquid chromatography (HPLC) and analyzed by an atmospheric pressure chemical ionization orbitrap mass spectrometer. Their study showed that low temperature oxidation at high pressure formed a highly complex species pool (for example hydroperoxides ($C_7H_{16}O_2$), keto-hydroperoxides ($C_7H_{14}O_3$), cyclic ethers ($C_7H_{14}O$), carboxylic acids ($C_2H_4O_2$, $C_3H_6O_2$, $C_4H_8O_2$), ketones ($C_{3-5}H_{6-10}O$), diones ($C_7H_{12}O_2$)), and highly oxygenated molecules ($C_7H_{14}O_5$, $C_7H_{14}O_7$, $C_7H_{14}O_9$, $C_7H_{14}O_{11}$) in *n*-heptane low temperature oxidation [20], indicating that current understanding of the low temperature oxidation mechanism and kinetic models require improvement. However, Dagaut's work is not online analysis, and chemical ionization makes quantification of the intermediates a challenge. An online measurement, comprehensive species analysis, and species quantification system is needed to study low temperature oxidation mechanism at high pressures.

This work develops a variable pressure jet-stirred reactor (VP-JSR) system working from one to ten bar, and couples the VP-JSR to the SVUV-PIMS at the Hefei Light Source. Molecular beam sampling was used to probe the reaction intermediates, which was analyzed by the SVUV-PIMS. This paper focuses on development of the sampling system, validation of the experimental setup, and a preliminary study of n-heptane low temperature oxidation from one to ten bar. The kinetic model of n-heptane low temperature oxidation by Zhang et al. [39] was used for comparison with the experimental data obtained in the present study.

2. Experimental method and kinetic modeling

The VP-JSR used in this work was similar to the high pressure JSR used in LRGP-CNRS [28]. The JSR is composed of fused silica, with a diameter of 52 mm and a volume of 65.4 cm^3. Thermocoax resistances were used to heat the preheating zone and the reactor. Temperature was monitored by K-type thermocouples fixed between the Thermocoax resistances and the

reactor wall. The temperature of the reaction was measured by another K-type thermocouple. The extremity of the thermocouple was located in the center of the reactor. From the outlet of the reactor, a thermocouple was inserted to measure the temperature distribution inside the JSR. Good temperature homogeneity was observed, except for a slight decrease of the temperature at the edge of the reactor outlet. The uncertainty of the reaction temperature measurement was estimated to be ±10 K.

In the experiment, the flow rate of the liquid fuel (e.g., *n*-heptane) was controlled by a HPLC plunger pump (model FL2200, Fuli Analytical Instruments Inc., Zhejiang, China); the flow rate of the gasses (O_2 and argon) was measured using MKS® mass flow controllers. The liquid was injected into a handmade vaporizer and vaporized at 373 K with argon as the dilution. Argon and O_2 were mixed and flowed into the preheating zone, and then to the reactor. The VP-JSR was set in a stainless-steel vessel; its pressure was adjustable from one to ten bar. Pressure was controlled by a needle valve. There were two holes with a diameter of 4 mm at the reactor outlet, to obtain the pressure balance between the inside and the outside of the VP-JSR. An auxiliary argon was made to flow into the steel vessel to flush the stainless-steel chamber.

The outlet of the JSR used in Hefei was shorter than the VP-JSR used in LRGP-CNRS; this modification was made to shorten the distance between the sampling nozzle and the edge of the reactor. The quartz nozzle could not resist the pressure difference of ca. ten bar in the ten bar experiment. Here, a stainless-steel nozzle was used for the sampling, as shown in Fig. 1a. The nozzle was coated by a Al_2O_3 layer to reduce catalytic reactions that could be caused by the metals in the stainless-steel nozzle.

The VP-JSR was coupled to two SVUV-PIMS systems at the Hefei Light Source. The first setup was installed at the combustion and flame beamline (BL03U). For this design, a three-stage sampling system was developed (Fig. 1b). This setup was used to study the low temperature oxidation of n-heptane at five and ten bar. The reaction products were first sampled using the stainless-steel nozzle, then the quartz nozzle, and finally to the nickel skimmer. The orifice

diameter of the stainless-steel nozzle, quartz nozzle and nickel skimmer was 50 μm, 250 μm, and two mm, respectively. Moreover, the direct simulation Monte Carlo (DSMC) method [40] was used to simulate the three-stage sampling system. The high mach number of argon expanding from the 50 μm stainless-steel nozzle (ca. 6 M) and the 250 μm nozzle (ca. 4 M) confirmed that the three-stage sampling system was molecular beam. Details of the simulation are provided in the Supplemental Material. For the one bar experiment, in the three-stage sampling the signal of the products was weak. The one bar experiment was conducted using two-stage sampling, as in the work of Herbinet et al. [41]. The mass resolution of the time-of-flight mass spectrometer (TOF-MS) at the combustion and flame beamline was ~2500 at m/z 40. For a better separation of the C/H/O composition of the low temperature oxidation intermediates, the five and ten bar experiment was also performed at the atomic and molecule physics beamline (BL09U). Mass spectra at selected temperatures were measured by TOF-MS with a mass resolution of ~4000 at m/z 40 [42]. In this experiment, the setup used two-stage sampling, as shown in Fig. 1c. Reaction products were first sampled using the stainless-steel nozzle, then directly to the nickel skimmer. The orifice diameters of the stainless-steel nozzle and the nickel skimmer were 50 μm and two mm, respectively. The one bar experiment at the atomic and molecule physics beamline was also repeated. Mole fraction profiles measured by the two setups were consistent.

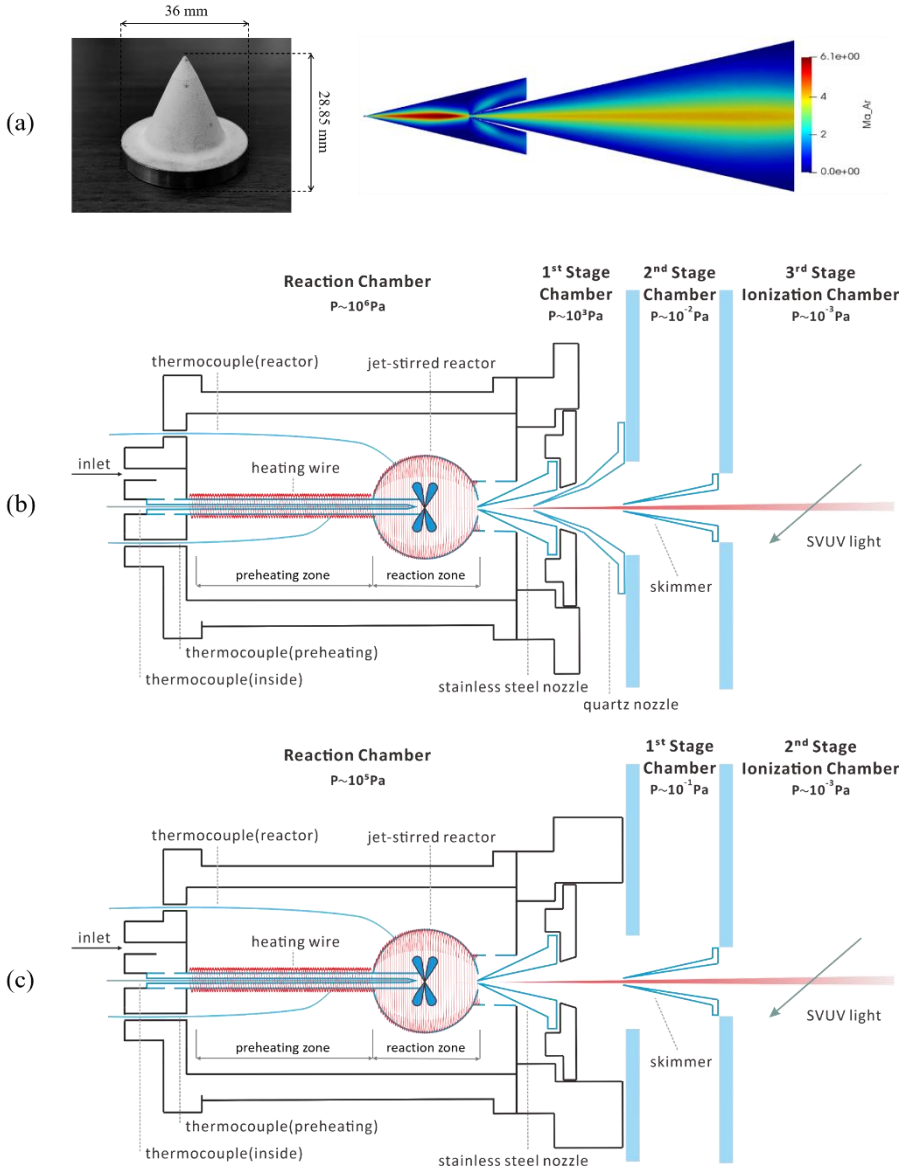

Figure 1. The stainless-steel nozzle with Al_2O_3 coating and the mach number distribution map of the Ar after the sampling by the 50 μm stainless steel nozzle and 250 μm quartz nozzle (a), the schematic of the VP-JSR coupled to the SVUV-PIMS system at Combustion and Flame beamline (b), and at Atomic and Molecule Physics beamline (c) of Hefei Light Source.

Experimental conditions of the *n*-heptane low temperature oxidation investigated in this work are shown in Table 2. The first and fourth series were performed under the same conditions as those used in Refs. [41] and [28], respectively, to validate the present setup. The data evaluation method of SVUV-PIMS was reported in previous work [41,43]. The mole fraction of the fuel was known at the unreacted temperature, its temperature-dependent mole fraction was calculated according to the corresponding signal and the gas expansion coefficient at each

temperature. The mole fraction of the products was then obtained with the fuel as a reference. Uncertainty for the quantified mole fraction was ±10% for the reactants, and ±20% for the species with a known photoionization cross section (PICS), and a factor of two for the species with unknown PICS. Mole fraction profiles discussed in this work are provided in the Supplementary Material. The *n*-heptane kinetic model by Zhang et al. [39] was used to simulate the experiment; simulation was performed using Chemkin-Pro-software with the perfect-stirred reactor (PSR) module [44]. Simulations were performed by fixing the reaction temperature, and the experimental conditions were used as input.

Table 2. The experimental conditions of *n*-heptane low-temperature oxidation. The highlighted conditions were used to validate the experimental setup.

Fuel	Pressure (bar)	Residence time (s)	Equivalence ratio	Fuel mole fraction	O_2 mole fraction
n-heptane	**1**	**2**	**1.0**	**0.005**	**0.0525**
	5	2	1.0	0.005	0.0525
	10	2	1.0	0.005	0.0525
	10	**2**	**1.0**	**0.001**	**0.0105**

3. Results and discussion

The experiment setup was first validated by comparison with *n*-heptane low-temperature oxidation data in the literature, as presented in Sections 3.1 and 3.2. Then, the *n*-heptane low-temperature oxidation at 1, 5, and 10 bar was carried out in this setup, as reported in Section 3.3. The reactivity of *n*-heptane oxidation, the species pool, and their distribution at different pressures are discussed. Furthermore, the prediction of the *n*-heptane kinetic model is compared to the newly obtained dataset and the observed deviations are discussed.

3.1 Validation of the setup at 1 bar

n-Heptane low temperature oxidation at one bar was studied by Herbinet et al. [41], with a fuel initial mole fraction of 0.005 and a residence time of 2 s. The experiment was repeated by Zhang et al. [39] in 2016, and Gao et al. [36] in 2019, using GC. Good agreement was observed among these three datasets, making these experimental conditions a good validation target for the present VP-JSR. In the Herbinet et al. data, both the GC and SVUV-PIMS were used to probe the low temperature oxidation intermediates. When GC data were not available in the following comparison, only the SVUV-PIMS data in Herbinet et al. are presented.

A comparison of mole fraction profiles of the fuel and typical low temperature oxidation intermediates is shown in Fig. 2. The measured *n*-heptane profile agreed well with the measurement of Herbinet et al. [41]. C_2H_4, CH_2O, and CH_3OH were quantified using the PICS measured by Cool et al. [45,46] and Dodson et al. [47]. They were in good agreement with Herbinet et al., considering the experimental uncertainty. The mole fraction for CH_2O, measured by CRDS in Rodriguez et al. [27], is also presented for comparison. The mole fraction measured by CRDS was slightly higher than the simulation and the PIMS measurement in this work. For the cyclic ether isomers ($C_7H_{14}O$), we presented the mole fraction profile of 2-ethyl-5-methyl tetrahydrofuran, measured by GC, the major component of the cyclic ether in n-heptane low temperature oxidation. The SVUV-PIMS data could not be quantified because their PICSs were unknown. The signal profile of $C_7H_{14}O$ measured by SVUV-PIMS was compared to the GC measured mole fraction.

The $C_7H_{12}O_2$, were likely to be the dione intermediate, with two keto groups, and were probably produced from the keto-hydroperoxides, or from the activated OOQOOH radical [8]. Like $C_7H_{14}O$, the $C_7H_{14}O_2$ was not quantified; its signal profile was presented for comparison. As shown in Fig. 2, the GC measured $C_7H_{12}O_2$ profile was different from the measurement by SVUV-PIMS in this work; this difference was also observed by Herbinet et al. [41]. These authors stated that GC measured $C_7H_{12}O_2$ may arise from decomposition of keto-hydroperoxide in the transfer

line between the JSR and the GC, because the GC measured $C_7H_{12}O_2$ had a temperature-dependent profile similar to the keto-hydroperoxide. The signal profile of $C_7H_{12}O_2$, measured by SVUV-PIMS in Herbinet et al., is also presented here; good agreement was observed for the two SVUV-PIMS data of $C_7H_{12}O_2$.

Peroxide intermediates such as H_2O_2 and keto-hydroperoxide ($C_7H_{14}O_3$), measured by SVUV-PIMS, are also presented in Fig. 2. H_2O_2 was quantified using the PICS reported by Dodson et al. [47]. In the *n*-heptane low temperature oxidation work by Rodriguez et al. [27], the mole fraction of H2O2 under the same experimental conditions was measured using continuous wave cavity ring-down spectroscopy (cw-CRDS). Although the temperature dependent profile of the two datasets was similar, there was a deviation factor of three for the mole fraction of H_2O_2. The source of the discrepancy was unclear, one possible reason was the uncertainty of the PICS of H_2O_2. The keto-hydroperoxide was not quantified; its signal profile is presented. The n-heptane low temperature model of Zhang et al. [39] satisfactorily predicted the measured species (mole fraction profile and signal profile) in Fig. 2, except that the reactivity of n-heptane from 500 to 600 K was slightly over-predicted; the mole fraction of ethylene and 2-ethyl-5-methyl tetrahydrofuran was over-predicted, and the mole fraction of $C_7H_{12}O_2$ dione was under-predicted.

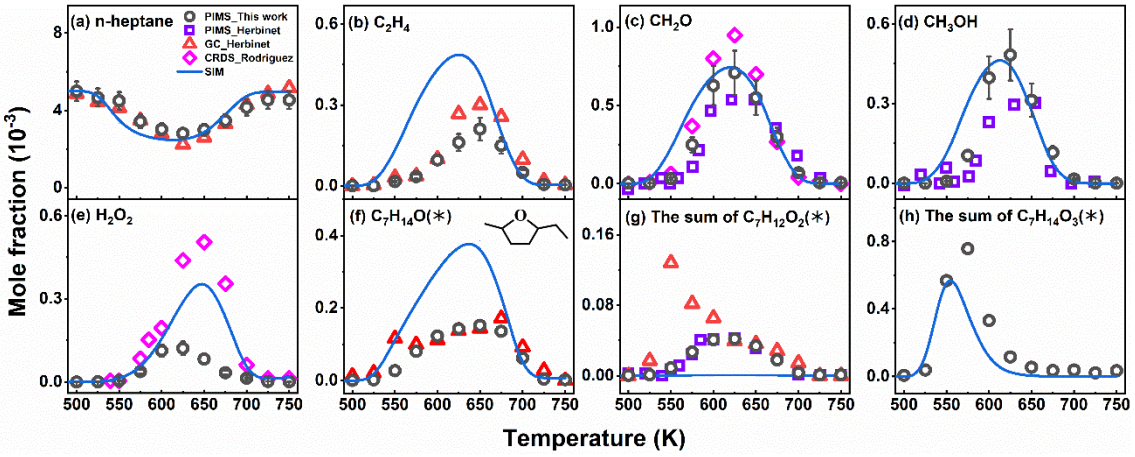

Figure 2. Data comparison of *n*-heptane low-temperature oxidation at 1 bar, in this work, with the measurement by Herbinet *et al.* [41] and Rodriguez *et al.* [27] (P = 1 bar, τ = 2 s, ϕ = 1.0 and x_{fuel}^{inlet} = 0.005). Error bar for the experimental data in this work is given. SVUV-PIMS data of $C_7H_{14}O$, $C_7H_{12}O_2$, and $C_7H_{14}O_3$ are signal profiles (*).

3.2 Validation of the setup at 10 bar

n-Heptane low temperature oxidation at ten bar was studied by Dagaut et al. [23], with the initial fuel mole fraction of 0.001, equivalence ratio of 1.0, and residence time of 1 s. Similar work was done by Herbinet et al. [28] at ten bar, with initial fuel mole fraction of 0.001, equivalence ratio of 1.0, and residence time of 2 s. The experiment by Herbinet et al. was repeated in this work. The experiment with 1 s residence time was not repeated because it required a total flow rate higher than 20 L/min., which exceeds the range of the mass flow controllers used in this work.

Table 3 presents the species pool measured by Dagaut et al., Herbinet et al., and this group. Here, only the molecular formula measured by GC and SVUV-PIMS was compared. It can be seen that the species pool measured by Dagaut et al. and Herbinet et.al. (mainly stable intermediates) was similar. The present SVUV-PIMS experiment not only probed these species but also a much more detailed species pool for the n-heptane low temperature oxidation at ten bar. They could be categorized into groups with a molecular formula of $C_7H_{14}O_x$ (x=0-3), $C_7H_{12}O_x$ (x=0-4), $C_7H_{10}O_x$ (x=0-4), C_nH_{2n} (n=2-6), C_nH_{2n-2} (n=2-6), $C_nH_{2n+2}O$ (n=1-3, 6), $C_nH_{2n}O$ (n=1-6), $C_nH_{2n-2}O$ (n=2-6), $C_nH_{2n-4}O$ (n=4-6), $C_nH_{2n+2}O_2$ (n=0-3, 7), $C_nH_{2n}O_2$ (n=1-4, 6), $C_nH_{2n-2}O_2$ (n=2-4), and $C_nH_{2n-4}O_2$ (n=4-5). This species pool was similar to that measured during the n-heptane low temperature oxidation at one bar in Ref. [17]. They were mainly alkenes, dienes, aldehyde/keto compounds, olefinic aldehyde/keto compounds, diones, cyclic ethers, peroxides, carboxylic acids, and alcohols/ethers. The free radicals were not studied in this work because they are quickly quenched at high pressure.

Table 3. Intermediate species measured during n-heptane oxidation in a JSR at 10 bar. The initial *n*-heptane mole fraction is 0.001, and equivalence ratio is 1.0. The measurements by Dagaut et al. [23] and Herbinet et al. [28] were performed using GC/GC–MS, while the measurement in this work was realized with SVUV-PIMS.

m/z	Dagaut	Herbinet	This work	m/z	Dagaut	Herbinet	This work
26	--	--	C_2H_2	86	$C_5H_{10}O$	--	$C_4H_6O_2/C_5H_{10}O$
28	C_2H_4	C_2H_4	C_2H_4	88	--	--	$C_4H_8O_2$
30	CH_2O	CH_2O	CH_2O	90	--	--	$C_4H_{10}O_2$
32	--	CH_4O	CH_4O	94	--	--	C_7H_{10}
34	--	--	H_2O_2	96	--	--	$C_7H_{12}/C_6H_8O/C_5H_4O_2$
40	--	--	C_3H_4	98	C_7H_{14}	C_7H_{14}	$C_7H_{14}/C_6H_{10}O/C_5H_6O_2$
42	C_3H_6	C_3H_6	C_3H_6/C_2H_2O	100	--	--	$C_6H_{12}O$
44	C_2H_4O	C_2H_4O	C_2H_4O	102	--	--	$C_6H_{14}O$
46	--	--	CH_2O_2/C_2H_6O	110	--	--	$C_7H_{10}O$
48	--	--	CH_4O_2	112	--	--	$C_7H_{12}O$
54	--	--	C_4H_6	114	$C_7H_{14}O$	$C_7H_{14}O$	$C_7H_{14}O$
56	C_4H_8/C_3H_4O	C_4H_8	C_4H_8/C_3H_4O	116	--	--	$C_6H_{12}O_2$
58	C_3H_6O	C_3H_6O	$C_3H_6O/C_2H_2O_2$	118	--	--	$C_5H_{10}O_3$
60	$C_2H_4O_2$	--	$C_2H_4O_2/C_3H_8O$	126	--	--	$C_7H_{10}O_2$
62	--	--	$C_2H_6O_2$	128	--	$C_7H_{12}O_2$	$C_7H_{12}O_2$
68	C_5H_8	--	C_5H_8/C_4H_4O	130	--	--	$C_7H_{14}O_2$
70	C_5H_{10}/C_4H_6O	C_5H_{10}	C_5H_{10}/C_4H_6O	132	--	--	$C_7H_{16}O_2$
72	C_4H_8O	C_4H_8O	$C_4H_8O/C_3H_4O_2$	140	--	--	$C_7H_8O_3$
74	--	--	$C_3H_6O_2$	142	--	--	$C_7H_{10}O_3$
76	--	--	$C_3H_8O_2$	144	--	--	$C_7H_{12}O_3$
80	--	--	C_6H_8	146	--	--	$C_7H_{14}O_3$
82	--	--	C_6H_{10}/C_5H_6O	158	--	--	$C_7H_{10}O_4$
84	C_6H_{12}	--	$C_6H_{12}/C_5H_8O/C_4H_4O_2$	160	--	--	$C_7H_{12}O_4$

Figure 3 shows the mole fraction profiles of *n*-heptane, O_2, CO, CO_2, H_2O, formaldehyde (CH_2O), acetaldehyde (C_2H_4O), methanol (CH_3OH), C_2H_4, C_3H_6, cyclic ethers ($C_7H_{14}O$) and diones ($C_7H_{14}O_2$) measured in this work, in Herbinet et al., and simulated by Zhang et al. In this work, the mole fraction of CO, CO_2, and O_2 was quantified by direct calibration with the standard gas. The PICS sources of formaldehyde, methanol, and C_2H_4 are given in Section 3.1. PICS for acetaldehyde and C_3H_6, were also measured by Cool et al. [45] and adopted in the mole fraction quantification. The mole fraction profiles of cyclic ether ($C_7H_{14}O$) are 2-ethyl-5-methyl

tetrahydrofuran. The mole fraction of diones ($C_7H_{14}O_2$), measured by GC, are the summation of the isomers, while the SVUV-PIMS signal profiles of these two intermediates are presented.

The two datasets were generally in good agreement for the selected species. *n*-Heptane and O_2 profiles in the NTC zone measured by Herbinet et al. were slightly lower than the measurement in this work, but the mole fraction profiles of the intermediates were not as different. The kinetic model satisfactorily predicted the mole fraction profiles of these species, except for CO_2, 2-ethyl-5-methyl tetrahydrofuran, and diones. The model over predicted the formation of 2-ethyl-5-methyl tetrahydrofuran at one bar (Fig. 2f) and ten bar. The rate of production (ROP) analysis showed that the reactions to forming 2-ethyl-5-methyl tetrahydrofuran were the same at both pressures, possibly because the branching ratio of QOOH cyclization to cyclic ether/the O_2 addition to QOOH radical was overestimated in the model. The $C_7H_{12}O_2$ diones were formed by two kinds of reactions in the model–the water elimination of the keto-hydroperoxides, and the subsequent reactions of the alkoxyl radicals (e.g., β-O-H elimination and bimolecular reaction with O_2) from keto-hydroperoxides decomposition. However, the model prediction of the $C_7H_{12}O_2$ diones was much lower than the experimental measurement, the simulated result was multiplied by a factor of 1000 to compare with the experimental measurement. The incomplete reaction pathways, such as the H-abstraction of keto-hydroperoxides [48,49], the reactions of the $C_7H_{14}O$ cyclic ethers [17], and the activated OOQOOH radical [8], may have contributed to the dione formation.

Furthermore, peroxide intermediates such as H_2O_2, methyl hydroperoxide, ethyl hydroperoxide, and the keto-hydroperoxides in n-heptane low temperature oxidation at ten bar were also measured by SVUV-PIMS (Fig. 4). Methyl hydroperoxide was quantified using photoionization cross calculated by Moshammer et al. [31]. Ethyl hydroperoxide and keto-hydroperoxides were not quantified, only their signal profiles are presented. The kinetic model satisfactorily predicted the mole fraction of methyl hydroperoxide, the signal profiles of ethyl hydroperoxide and keto-hydroperoxides. However, the mole fraction of H_2O_2 was overestimated.

As discussed above, the H_2O_2 mole fraction measured at one bar by SVUV-PIMS was a factor of three lower than the cw-CRDS measurement. If the mole fraction is multiplied by a factor of three, it is close to the simulation at 650 K. However, the model predicted a rapid formation of H_2O_2 from 750 to 800 K, while the experiment did not behave this way.

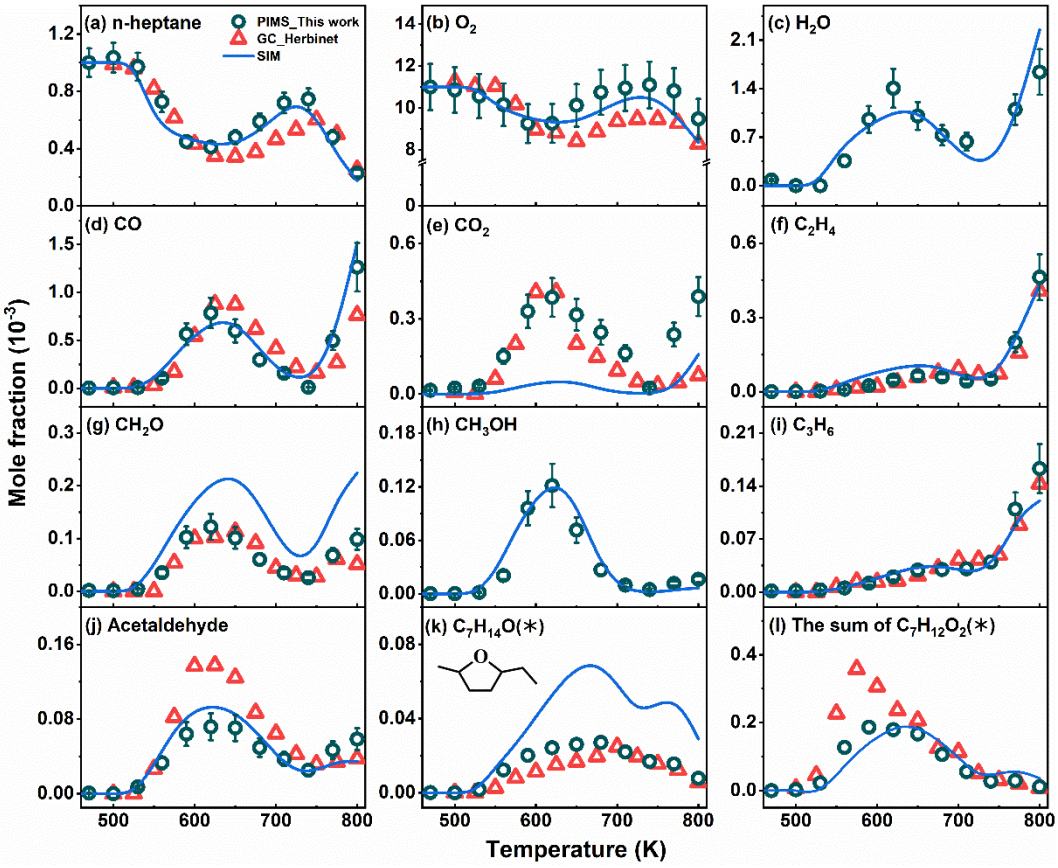

Figure 3. Comparison of data of *n*-heptane low-temperature oxidation at 10 bar measured in this work, by Herbinet *et al*. [28], and by the simulation of Zhang *et al*. [39] (P = 10 bar, τ = 2 s, ϕ = 1.0 and x_{fuel}^{inlet} = 0.001). Simulated mole fraction of $C_7H_{12}O_2$ in (l) is multiplied by a factor of 1000. Error bar for the experimental data in this work is given. We note that the SVUV-PIMS data for $C_7H_{14}O$ and $C_7H_{12}O_2$ is signal profile (*) scaled to match the mole fraction profile measured by GC.

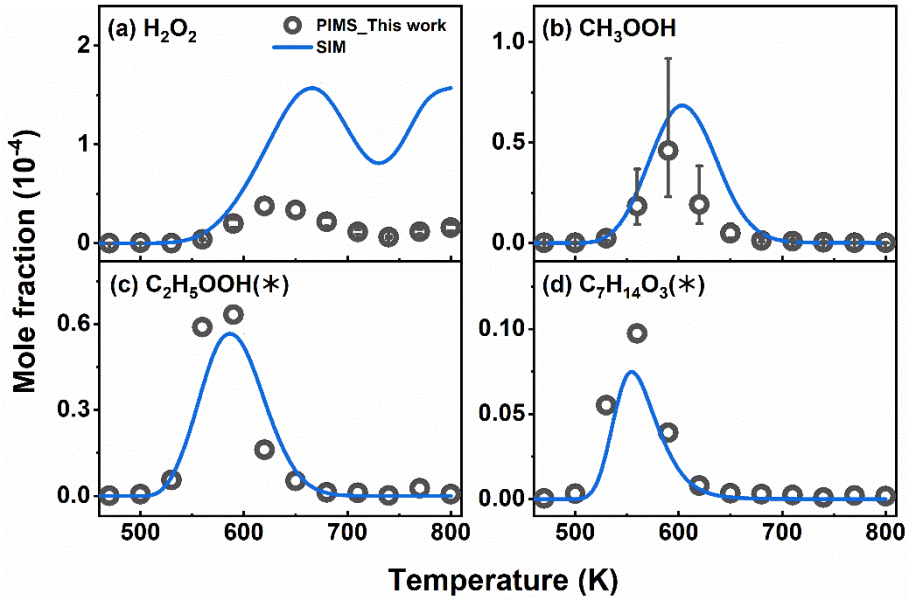

Figure 4. Experimental (symbols) and simulated (lines) profiles of H_2O_2 (a), methyl hydroperoxide (b), ethyl hydroperoxide (c), and keto-hydroperoxides (d) in *n*-heptane low-temperature oxidation (P = 10 bar, τ = 2 s, ϕ = 1.0 and x_{fuel}^{inlet} = 0.001). Error bar for the experimental data in this work is given. The signal profiles (*) of ethyl hydroperoxide and keto-hydroperoxides are presented.

3.3 *n*-heptane low-temperature oxidation from 1 to 10 bar

Discussions in Sections 3.1 and 3.2 establish that the VP-JSR, coupled to the SVUV-PIMS system, is a new tool suitable to study low temperature oxidation chemistry. Using this design, we studied the low temperature oxidation of *n*-heptane at one, five and ten bar, to evaluate the pressure effect on low temperature oxidation. The experimental conditions are shown in Table 2, i.e., *n*-heptane initial mole fraction of 0.005, residence time of 2 s, and equivalence ratio of 1.0. The result showed that oxidations at one, five and ten bar had similar species categories/identification, but showed strong differences in reactivity and in the distribution of the mole fraction profiles, presented in the discussion to follow.

Figure 5 compares temperature-dependent profiles of reactants, final products, and initial oxidation intermediates of *n*-heptane from one to ten bar. The mole fraction of *n*-heptane, O_2, CO,

CO_2, and H_2O was quantified; the mole fraction of keto-hydroperoxides was not quantified because its PICS was unknown. Here, their relative ratio at one, five and ten bar is displayed by normalizing their signal with the initial signal of n-heptane (i.e., at 500 K) at 11.5 eV photon energy.

From one to ten bar, reactivity was promoted in both the initial reaction temperature and the conversion of the fuel. The higher reactivity, between 550 and 600 K, increased reaction reactivity further in the negative temperature coefficient (NTC) zone. Compared to the one bar experiment, the five and ten bar low temperature oxidation showed weak NTC behavior. Higher reactivity was also indicated by the formation of CO, H_2O, CO_2, C_2H_4, and C_3H_6, especially in the 650–770 K range. The higher reactivity between 550 and 600 K at higher pressure was also confirmed by the higher formation of keto-hydroperoxides. At five and ten bar, the initial formation temperature of the keto-hydroperoxides was lower than that at one bar; higher pressure also promoted the formation of the keto-hydroperoxides, as shown in Fig. 5h. The kinetic model satisfactorily predicted the pressure effect on the conversion of *n*-heptane and O_2, and the formation of CO, H_2O, C_2H_4, and keto-hydroperoxides. It was noted that the temperature corresponding to the maximum mole fraction of keto-hydroperoxides was on the order of one bar > five bar > ten bar, but the model prediction at ten bar was slightly higher than the measurement. Moreover, the model under predicted the formation of CO_2 (Fig. 5d) and over predicted the formation of formaldehyde (Fig. 5g) at five and ten bar. These two intermediates involved in the reactions of the base model–and a thorough analysis of the mechanism–is needed in future work.

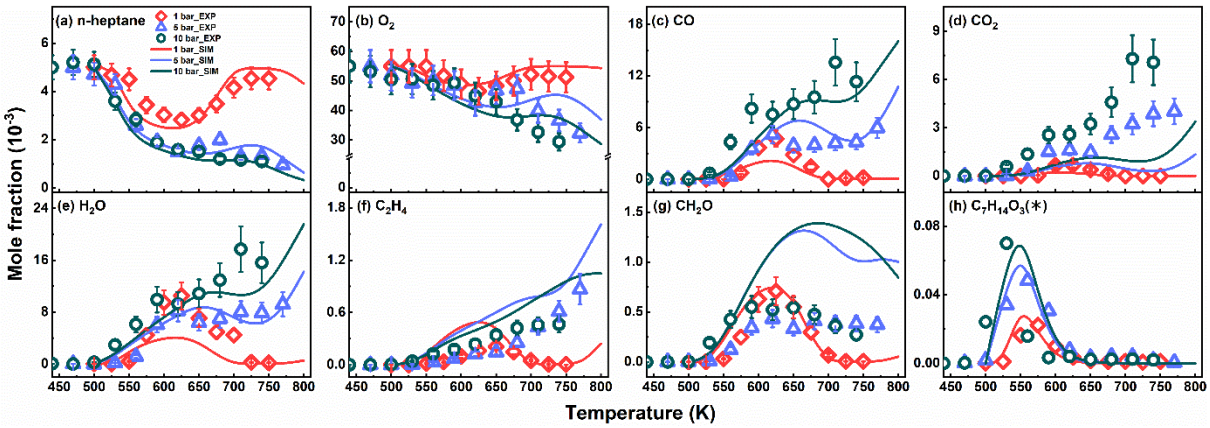

Figure 5. Experimental (symbols) and simulated (lines) profile of *n*-heptane, O_2, CO, CO_2, H_2O, C_2H_4, CH_2O, and keto-hydroperoxides in *n*-heptane low-temperature oxidation (P = 1, 5, and 10 bar, τ = 2 s, ϕ = 1.0 and x_{fuel}^{inlet} = 0.005). Error bar for the experimental data in this work is given. Signal profile (*) of keto-hydroperoxides is presented.

The pressure effect on the formation of H_2O_2 and formic acid is shown in Fig. 6. The experiment proved that formation of H_2O_2 was promoted when the pressure was increased from one to ten bar. The promoting effect of increased pressure on H_2O_2 formation was predicted well by the simulation, however, the kinetic model significantly over predicted the mole fraction of H_2O_2 (Fig. 6a). A large difference was observed in the NTC zone at five and ten bar (ca. a factor of 20 at 750 K). The ROP analysis revealed that H_2O_2 was predominantly formed from the self-reaction of HO_2 radicals at 750 K, which was related to the reactions in the base model, such as HCO, CH_2O, CH_3O, and CH_3O_2. Evaluating these reactions in the base model is outside the scope of this work.

The experiments showed no apparent pressure effect on the formation of formic acid from one to ten bar, while such an effect was not predicted by the simulation, where a significant promotion of formic acid formation at five and ten bar was observed. Also, the mole fraction of formic acid was over predicted by a factor of five, nine, and 11 at one, five and ten bar, respectively. ROP analysis showed that formic acid was predominantly formed from the following reaction

steps:

$CH_2O + OH = HOCH_2O$ (R1)

$HOCH_2O = HOCHO + H$ (R2)

As mentioned by Wang et al. [17], the rate constant of R1 in the model was overestimated by adopting the rate constant from Taylor et al. [50]. This caused high carbon flux to formic acid and explained the overestimation of formic acid at one, five and ten bar. Furthermore, our experiment showed a slight effect of pressure on the formation of formaldehyde (Fig. 5g), but the model predicted that the formation of formaldehyde was promoted at five and ten bar, which further promoted formic acid formation at five and ten bar (Fig. 6b).

The pressure effect on the formation of $C_7H_{12}O_2$ intermediate is shown in Fig. 7. The GC measurement by Herbinet et al. [28] measured two dione intermediates (i.e., 2,4-heptadione and 3,5-heptadione) during *n*-heptane low temperature at ten bar. The mole fraction of 2,4-heptadione was much higher than that of 3,5-heptadione. In this work, it was not possible to separate the isomers or to quantify them. The relative ratio of the total $C_7H_{12}O_2$ in Fig. 7 revealed that the effect of pressure on its formation was negligible. This observation was contrary to the conclusion of Herbinet et al. [28], who stated that high pressure promoted the formation of diones. The simulation for the $C_7H_{12}O_2$ diones in Fig. 7 also indicated that high pressure was favorable for dione formation. One possible explanation is that the SVUV-PIMS signal of $C_7H_{12}O_2$ included other intermediates, such as isomers with a carbonyl and a cyclic ether functional group, proposed by Wang et al. [17].

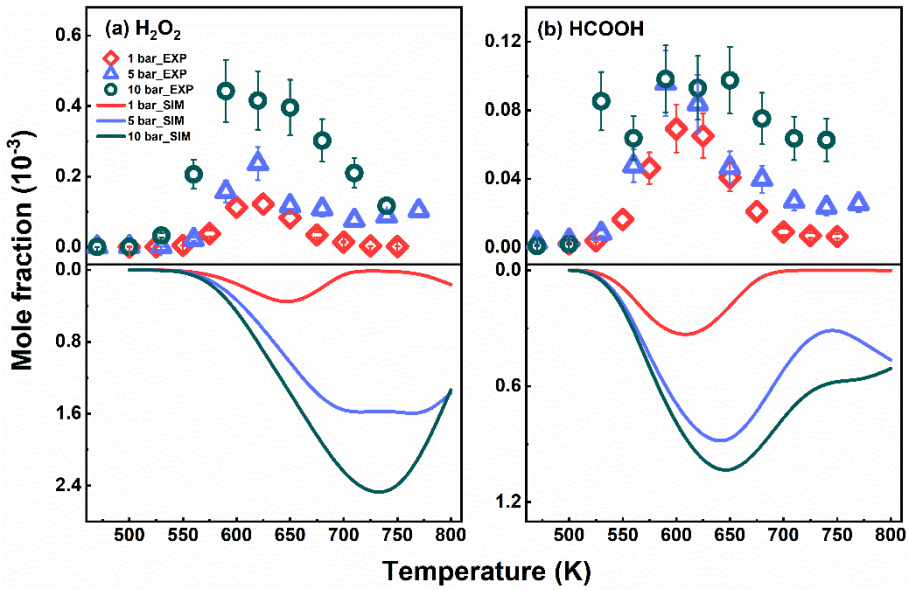

Figure 6. Experimental (symbols) and simulated (lines) profile of H_2O_2 and formic acid in *n*-heptane low-temperature oxidation (P = 1, 5, and 10 bar, τ = 2 s, ϕ = 1.0 and x_{fuel}^{inlet} = 0.005). Error bar for the experimental data in this work is given.

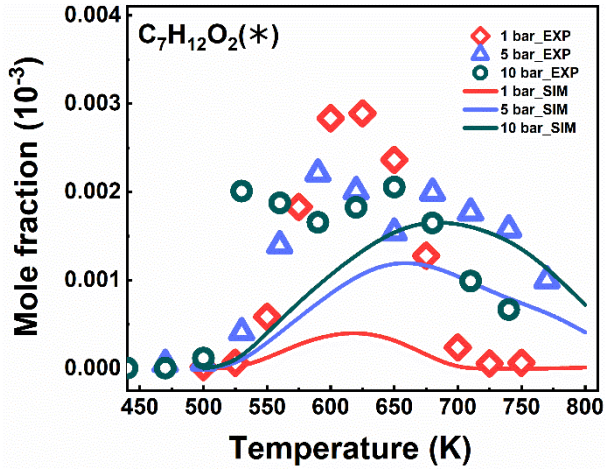

Figure 7. Experimental (symbols) and simulated (lines) profile of $C_7H_{12}O_2$ in *n*-heptane low-temperature oxidation (P = 1, 5, and 10 bar, τ = 2 s, ϕ = 1.0 and x_{fuel}^{inlet} = 0.005). Signal profile (*) of $C_7H_{12}O_2$ is presented.

4. Summary and conclusion

In this work a variable pressure JSR (up to ten bar) system was developed, which adopted the molecular beam sampling and synchrotron radiation photoionization mass spectrometry for species identification and quantification. The setup was validated by repeating experiments on the low temperature oxidation of n-heptane at one and ten bar. The good agreement between the data from this work and in the literature showed that the VP-JSR system is suitable for study of low temperature oxidation chemistry. Compared to customary JSR systems that use GC, GC–MS, and FTIR to measure low temperature oxidation products, the molecular beam sampling, coupled with synchrotron vacuum ultraviolet photoionization mass spectrometry, produced a more comprehensive measurement of the intermediates–especially the peroxides, carboxylic acids, and oxygenated intermediates with multiple functional groups. The development of the VP-JSR-SVUV-PIMS setup in this work is useful to the study of low temperature oxidation mechanisms, providing a comprehensive dataset for examining chemical kinetic models. The kinetic model of Zhang et al. could predict n-heptane low temperature oxidation at one, five and ten bar, but needs to improve the reaction mechanism for some specific species, especially hydrogen peroxide, formic acid, carbon dioxide, the cyclic ether, and the dione intermediates. A detailed analysis of the pressure effect on the low temperature oxidation could be the goal of future work.

Acknowledgements

This work was supported by National Natural Science Foundation of China (51976208, 61871172), by Hefei Science Center，CAS (2020HSC-KPRD001), and by the DNL Cooperation Fund, CAS (DNL202005).

References

[1] M. Yao, Z. Zheng, H. Liu, Progress and recent trends in homogeneous charge compression ignition (HCCI) engines, Prog. Energy Combust. Sci. 35 (2009) 398-437.

[2] S. Saxena, I.D. Bedoya, Fundamental phenomena affecting low temperature combustion and HCCI engines, high load limits and strategies for extending these limits, Prog. Energy Combust. Sci. 39 (2013) 457-488.

[3] N. Kurimoto, B. Brumfield, X. Yang, T. Wada, P. Diévart, G. Wysocki, Y. Ju, Quantitative measurements of HO_2/H_2O_2 and intermediate species in low and intermediate temperature oxidation of dimethyl ether, Proc. Combust. Inst. 35 (2015) 457-464.

[4] H. Guo, W. Sun, F.M. Haas, T. Farouk, F.L. Dryer, Y. Ju, Measurements of H_2O_2 in low temperature dimethyl ether oxidation, Proc. Combust. Inst. 34 (2013) 573-581.

[5] R.K. Hanson, D.F. Davidson, Recent advances in laser absorption and shock tube methods for studies of combustion chemistry, Prog. Energy Combust. Sci. 44 (2014) 103-114.

[6] C.-J. Sung, H.J. Curran, Using rapid compression machines for chemical kinetics studies, Prog. Energy Combust. Sci. 44 (2014) 1-18.

[7] O. Herbinet, F. Battin-Leclerc, Progress in Understanding Low-Temperature Organic Compound Oxidation Using a Jet-Stirred Reactor, Int. J. Chem. Kinet. 46 (2014) 619-639.

[8] Z. Wang, O. Herbinet, N. Hansen, F. Battin-Leclerc, Exploring hydroperoxides in combustion: History, recent advances and perspectives, Prog. Energy Combust. Sci. 73 (2019) 132-181.

[9] P. Dagaut, M. Cathonnet, J.P. Rouan, R. Foulatier, A. Quilgars, J.C. Boettner, F. Gaillard, H. James, A jet-stirred reactor for kinetic studies of homogeneous gas-phase reactions at pressures up to ten atmospheres (1 MPa), J. Phys. E: Sci. Instrum. 19 (1986) 207–209.

[10] F. Qi, Combustion chemistry probed by synchrotron VUV photoionization mass spectrometry, Proc. Combust. Inst. 34 (2013) 33-63.

[11] H. Zhao, C. Yan, T. Zhang, G. Ma, M.J. Souza, C.-w. Zhou, Y. Ju, Studies of high-pressure n-butane oxidation with CO_2 dilution up to 100 atm using a supercritical-pressure jet-stirred reactor, Proc. Combust. Inst. 38 (2021) 279-287.

[12] C. Bahrini, O. Herbinet, P.-A. Glaude, C. Schoemaecker, C. Fittschen, F. Battin-Leclerc, Quantification of Hydrogen Peroxide during the Low-Temperature Oxidation of Alkanes, J. Am. Chem. Soc. 134 (2012) 11944-11947.

[13] M. Djehiche, N.L. Le Tan, C.D. Jain, G. Dayma, P. Dagaut, C. Chauveau, L. Pillier, A. Tomas, Quantitative Measurements of HO_2 and Other Products of n-Butane Oxidation (H_2O_2, H_2O, CH_2O, and C_2H_4) at Elevated Temperatures by Direct Coupling of a Jet-Stirred Reactor with Sampling Nozzle and Cavity Ring-Down Spectroscopy (cw-CRDS), J. Am. Chem. Soc. 136 (2014) 16689-16694.

[14] A. Rodriguez, O. Herbinet, Z. Wang, F. Qi, C. Fittschen, P.R. Westmoreland, F. Battin-Leclerc, Measuring hydroperoxide chain-branching agents during n-pentane low-temperature oxidation, Proc. Combust. Inst. 36 (2017) 333-342.

[15] Z. Zhou, X. Du, J. Yang, Y. Wang, C. Li, S. Wei, L. Du, Y. Li, F. Qi, Q. Wang, The vacuum ultraviolet beamline/endstations at NSRL dedicated to combustion research, J. Synchrotron Radiat. 23 (2016) 1035-1045.

[16] K. Moshammer, A.W. Jasper, D.M. Popolan-Vaida, A. Lucassen, P. Diévart, H. Selim, A.J. Eskola, C.A. Taatjes, S.R. Leone, S.M. Sarathy, Y. Ju, P. Dagaut, K. Kohse-Höinghaus, N. Hansen, Detection and Identification of the Keto-Hydroperoxide ($HOOCH_2OCHO$) and Other Intermediates during Low-Temperature Oxidation of Dimethyl Ether, J. Phys. Chem. A 119 (2015) 7361-7374.

[17] Z. Wang, B. Chen, K. Moshammer, D.M. Popolan-Vaida, S. Sioud, V.S.B. Shankar, D. Vuilleumier, T. Tao, L. Ruwe, E. Bräuer, N. Hansen, P. Dagaut, K. Kohse-Höinghaus, M.A. Raji, S.M. Sarathy, n-Heptane cool flame chemistry:

Unraveling intermediate species measured in a stirred reactor and motored engine, Combust. Flame 187 (2018) 199-216.

[18] Z. Wang, D.M. Popolan-Vaida, B. Chen, K. Moshammer, S. Mohamed, H. Wang, S. Sioud, M.A. Raji, K. Kohse-Höinghaus, N. Hansen, P. Dagaut, S.R. Leone, Sarathy, S. Mani, Unraveling the structure and chemical mechanisms of highly oxygenated intermediates in oxidation of organic compounds, Proc. Natl. Acad. Sci. U.S.A. 114 (2017) 13102–13107.

[19] N. Belhadj, R. Benoit, P. Dagaut, M. Lailliau, Z. Serinyel, G. Dayma, F. Khaled, B. Moreau, F. Foucher, Oxidation of di-n-butyl ether: Experimental characterization of low-temperature products in JSR and RCM, Combust. Flame 222 (2020) 133-144.

[20] N. Belhadj, R. Benoit, P. Dagaut, M. Lailliau, Experimental characterization of n-heptane low-temperature oxidation products including keto-hydroperoxides and highly oxygenated organic molecules (HOMs), Combust. Flame 224 (2021) 83-93.

[21] F. Battin-Leclerc, J. Bourgalais, Z. Gouid, O. Herbinet, G. Garcia, P. Arnoux, Z. Wang, L.-S. Tran, G. Vanhove, L. Nahon, M. Hochlaf, Chemistry deriving from OOQOOH radicals in alkane low-temperature oxidation: A first combined theoretical and electron-ion coincidence mass spectrometry study, Proc. Combust. Inst. 38 (2021) 309-319.

[22] J. Bourgalais, Z. Gouid, O. Herbinet, G.A. Garcia, P. Arnoux, Z. Wang, L.-S. Tran, G. Vanhove, M. Hochlaf, L. Nahon, F. Battin-Leclerc, Isomer-sensitive characterization of low temperature oxidation reaction products by coupling a jet-stirred reactor to an electron/ion coincidence spectrometer: case of n-pentane, Phys. Chem. Chem. Phys 22 (2020) 1222-1241.

[23] P. Dagaut, M. Reuillon, M. Cathonnet, Experimental study of the oxidation of *n*-heptane in a jet stirred reactor from low to high temperature and pressures up to 40 atm, Combust. Flame 101 (1995) 132-140.

[24] M. Carbonnier, Z. Serinyel, A. Kéromnès, G. Dayma, B. Lefort, L. Le Moyne, P. Dagaut, An experimental and modeling study of the oxidation of 3-pentanol at high pressure, Proc. Combust. Inst. 37 (2019) 477-484.

[25] C.A.R. Pappijn, N. Vin, F.H. Vermeire, R. Van de Vijver, O. Herbinet, F. Battin-Leclerc, M.-F. Reyniers, G.B. Marin, K.M. Van Geem, Experimental and kinetic modeling study of the pyrolysis and oxidation of diethylamine, Fuel 275 (2020) 117744.

[26] C. Bahrini, O. Herbinet, P.-A. Glaude, C. Schoemaecker, C. Fittschen, F. Battin-Leclerc, Detection of some stable species during the oxidation of methane by coupling a jet-stirred reactor (JSR) to cw-CRDS, Chem. Phys. Lett. 534 (2012) 1-7.

[27] A. Rodriguez, O. Herbinet, X. Meng, C. Fittschen, Z. Wang, L. Xing, L. Zhang, F. Battin-Leclerc, Hydroperoxide Measurements During Low-Temperature Gas-Phase Oxidation of n-Heptane and n-Decane, J. Phys. Chem. A 121 (2017) 1861-1876.

[28] O. Herbinet, B. Husson, H. Le Gall, F. Battin-Leclerc, An experimental and modeling study of the oxidation of n-heptane, ethylbenzene, and n-butylbenzene in a jet-stirred reactor at pressures up to 10 bar, Int. J. Chem. Kinet. 52 (2020) 1006-1021.

[29] O. Herbinet, B. Husson, H. Le Gall, F. Battin-Leclerc, Comparison study of the gas-phase oxidation of alkylbenzenes and alkylcyclohexanes, Chem. Eng. Sci. 131 (2015) 49-62.

[30] B. Chen, Z. Wang, J.-Y. Wang, C. Togbé, P.E. Álvarez Alonso, M. Almalki, M. Mehl, W.J. Pitz, S.W. Wagnon, K. Zhang, G. Kukkadapu, P. Dagaut, S.M. Sarathy, Exploring gasoline oxidation chemistry in jet stirred reactors, Fuel 236 (2017) 1282-1292.

[31] K. Moshammer, A.W. Jasper, D.M. Popolan-Vaida, Z. Wang, V.S. Bhavani Shankar, L. Ruwe, C.A. Taatjes, P. Dagaut, N. Hansen, Quantification of the Keto-Hydroperoxide ($HOOCH_2OCHO$) and Other Elusive Intermediates during Low-Temperature Oxidation of Dimethyl Ether, J. Phys. Chem. A 120 (2016) 7890–7901.

[32] Z. Wang, L. Zhang, K. Moshammer, D.M. Popolan-Vaida, V.S. Bhavani Shankar, A. Lucassen, C. Hemken, C.A.

Taatjes, S.R. Leone, K. Kohse-Höinghaus, N. Hansen, P. Dagaut, S.M. Sarathy, Additional chain-branching pathways in the low-temperature oxidation of branched alkanes, Combust. Flame 164 (2016) 386-396.

[33] O. Herbinet, F. Battin-Leclerc, S. Bax, H.L. Gall, P.-A. Glaude, R. Fournet, Z. Zhou, L. Deng, H. Guo, M. Xie, F. Qi, Detailed product analysis during the low temperature oxidation of *n*-butane, Phys. Chem. Chem. Phys 13 (2011) 296-308.

[34] B.-Y. Wang, Y.-X. Liu, J.-J. Weng, P. Glarborg, Z.-Y. Tian, New insights in the low-temperature oxidation of acetylene, Proc. Combust. Inst. 36 (2017) 355-363.

[35] J. Zou, H. Jin, D. Liu, X. Zhang, H. Su, J. Yang, A. Farooq, Y. Li A comprehensive study on low-temperature oxidation chemistry of cyclohexane. II. Experimental and kinetic modeling investigation, Combust. Flame In press, 10.1016/j.combustflame.2021.111550 (2021).

[36] Z. Gao, E. Hu, Z. Xu, G. Yin, Z. Huang, Low to intermediate temperature oxidation studies of dimethoxymethane/n-heptane blends in a jet-stirred reactor, Combust. Flame 207 (2019) 20-35.

[37] G. Yin, J. Xu, E. Hu, Q. Gao, H. Zhan, Z. Huang, Experimental and kinetic study on the low temperature oxidation and pyrolysis of formic acid in a jet-stirred reactor, Combust. Flame 223 (2021) 77-87.

[38] N. Belhadj, R. Benoit, P. Dagaut, M. Lailliau, Experimental Characterization of Tetrahydrofuran Low-Temperature Oxidation Products Including Ketohydroperoxides and Highly Oxygenated Molecules, Energy Fuels 35 (2021) 7242-7252.

[39] K. Zhang, C. Banyon, J. Bugler, H.J. Curran, A. Rodriguez, O. Herbinet, F. Battin-Leclerc, C. B'Chir, K.A. Heufer, An updated experimental and kinetic modeling study of *n*-heptane oxidation, Combust. Flame 172 (2016) 116-135.

[40] G.A. Bird, Approach to Translational Equilibrium in a Rigid Sphere Gas, Phys. Fluids 6 (1963) 1518.

[41] O. Herbinet, B. Husson, Z. Serinyel, M. Cord, V. Warth, R. Fournet, P.-A. Glaude, B. Sirjean, F. Battin-Leclerc, Z. Wang, M.F. Xie, Z.J. Cheng, F. Qi, Experimental and modeling investigation of the low-temperature oxidation of *n*-heptane, Combust. Flame 159 (2012) 3455-3471.

[42] Q. Xu, B. Liu, W. Chen, T. Yu, Z. Zhang, C. Zhang, L. Wei, Z. Wang, Comprehensive study of the low-temperature oxidation chemistry by synchrotron photoionization mass spectrometry and gas chromatography, Combust. Flame 236 (2022) 111797.

[43] Z. Wang, O. Herbinet, Z. Cheng, B. Husson, R. Fournet, F. Qi, F. Battin-Leclerc, Experimental Investigation of the Low Temperature Oxidation of the Five Isomers of Hexane, J. Phys. Chem. A 118 (2014) 5573-5594.

[44] CHEMKIN-PRO 15112, Reaction Design: San Diego, (2012).

[45] T.A. Cool, K. Nakajima, T.A. Mostefaoui, F. Qi, A. McIlroy, P.R. Westmoreland, M.E. Law, L. Poisson, D.S. Peterka, M. Ahmed, Selective detection of isomers with photoionization mass spectrometry for studies of hydrocarbon flame chemistry, J. Chem. Phys. 119 (2003) 8356-8365.

[46] T.A. Cool, J. Wang, K. Nakajima, C.A. Taatjes, A. McIlroy, Photoionization cross sections for reaction intermediates in hydrocarbon combustion, Int. J. Mass Spectrom. 247 (2005) 18-27.

[47] L.G. Dodson, L. Shen, J.D. Savee, N.C. Eddingsaas, O. Welz, C.A. Taatjes, D.L. Osborn, S.P. Sander, M. Okumura, VUV Photoionization Cross Sections of HO_2, H_2O_2, and H_2CO, J. Phys. Chem. A 119 (2015) 1279-1291.

[48] E. Ranzi, C. Cavallotti, A. Cuoci, A. Frassoldati, M. Pelucchi, T. Faravelli, New reaction classes in the kinetic modeling of low temperature oxidation of *n*-alkanes, Combust. Flame 162 (2015) 1679–1691.

[49] L. Xing, J.L. Bao, Z. Wang, F. Zhang, D.G. Truhlar, Degradation of Carbonyl Hydroperoxides in the Atmosphere and in Combustion, J. Am. Chem. Soc. 139 (2017) 15821-15835.

[50] P.H. Taylor, M.S. Rahman, M. Arif, B. Dellinger, P. Marshall, Kinetic and mechanistic studies of the reaction of hydroxyl radicals with acetaldehyde over an extended temperature range, Proc. Combust. Inst. 26 (1996) 497-504.